

## Magnetic Bistability in a Discrete Organic Radical

Tao Li,<sup>†</sup> Gengwen Tan,<sup>†</sup> Dong Shao,<sup>†</sup> Jing Li,<sup>†</sup> Zaichao Zhang,<sup>‡</sup> You Song,<sup>†</sup> Yunxia Sui,<sup>§</sup> Sheng Chen,<sup>†</sup> Yong Fang,<sup>†</sup> and Xinping Wang<sup>\*,†</sup>

<sup>†</sup>State Key Laboratory of Coordination Chemistry, School of Chemistry and Chemical Engineering, Collaborative Innovation Center of Advanced Microstructures and <sup>§</sup>Centre of Modern Analysis, Nanjing University, Nanjing 210023, China

<sup>‡</sup>School of Chemistry and Chemical Engineering, Huaiyin Normal University, Huai'an 223300, China

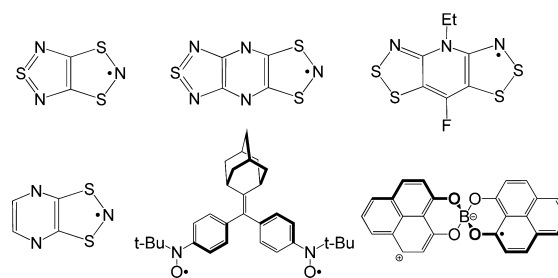
### Supporting Information

**ABSTRACT:** Molecular assembly with magnetic bistability has been of considerable interest for application as electronic devices. In contrast to transition-metal complexes, magnetic bistability so far observed in organic radical crystals is mainly caused by intermolecular electron-exchange interaction. We now report that the magnetic bistability in an organic radical can also be caused by intramolecular electron-exchange interaction. The diradical salt of 1,4-di(bisphenylamino)-2,3,5,6-tetramethylbenzene undergoes a phase transition with a thermal hysteresis loop over the temperature range from 118 to 131 K. The phases above and below the loop correspond to two different singlet states of the diradical dication. The results provide a novel organic radical material as an unprecedented instance of an intramolecular magnetic bistability revalent to the design of functional materials.

Preparation and solid-state properties (electrical, optical, and magnetic, etc.) of organic radicals have been extensively studied.<sup>1</sup> The use of organic radicals as building blocks for functional molecular materials has aroused a growing interest.<sup>1</sup> These materials often exhibit molecular bistability, i.e., the property of materials exist in two interchangeable phases by external stimuli (temperature, pressure, light, etc.), which has been of considerable interest for application as electronic devices, such as thermal sensors, switching devices and information storage.<sup>2–6</sup> Magnetic bistability has been widely observed in a discrete paramagnetic transition metal complex.<sup>7</sup> The bistable crystalline organic radicals so far known (Scheme 1), however, are based on radical stacks or dimers, and their magnetic bistability is mainly caused by intermolecular electron-exchange interactions.<sup>2–6</sup> In many cases, they undergo a spin transition between a radical ( $S = 1/2$ ) and a  $\pi/\sigma$ -dimer ( $S = 0$ ).<sup>2–5</sup> Magnetic bistability in a discrete organic radical, induced by intramolecular electron-exchange interaction, has not yet been observed experimentally.

Recently, we and others have prepared a series of stable nitrogen-incorporating diradical dications,<sup>8,9</sup> analogues of pure organic diradicals such as Thiele's and Chichibabin's hydrocarbons.<sup>10</sup> During the synthesis of their derivative, diradical dication of 1,4-di(bisphenylamino)-2,3,5,6-tetramethylbenzene ( $I^{2+}$ ), we observed that intramolecular electron-exchange interaction can cause a hysteresis loop, which is the first instance of magnetic bistability in a discrete organic radical.

### Scheme 1. Representative Crystalline Organic Radicals with Magnetic Bistability Induced by Intermolecular Electron-Exchange Interaction

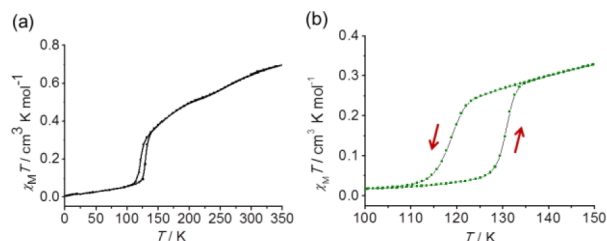
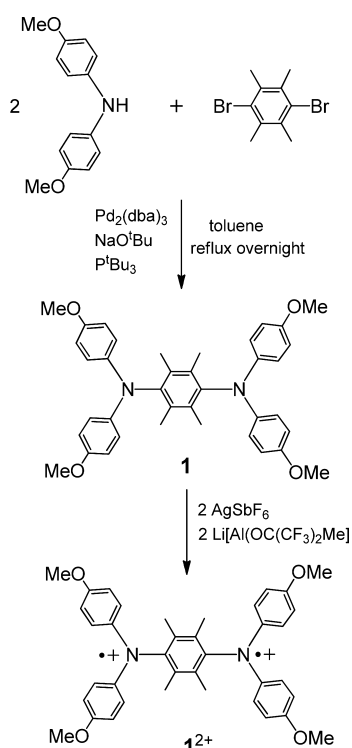


Standard Buchwald–Hartwig amination of 1,4-dibromotetramethylbenzene with di-*p*-methoxyphenylamine in the presence of sodium *tert*-butoxide in reflux toluene afforded compound **1** as white solid (Scheme 2). Cyclic voltammetry (CV) of **1** in  $\text{CH}_2\text{Cl}_2$  at room temperature with  ${}^t\text{Bu}_4\text{NPF}_6$  as a supporting electrolyte revealed a quasi-reversible two-electron oxidation peak at oxidation potential of +0.61 V (see Figure S1). Upon oxidation with 2 molar equiv of  $\text{AgSbF}_6$  and  $\text{Li}[\text{Al}(\text{OR}_{\text{Me}})_4]$  ( $\text{OR}_{\text{Me}} = \text{OC}(\text{CF}_3)_2\text{Me}$ )<sup>11</sup> in  $\text{CH}_2\text{Cl}_2$ , the neutral precursor **1** was converted to dication  $I^{2+}$  in a high yield, accompanied by precipitates of Ag metal and  $\text{LiSbF}_6$ . The resultant dication is thermally stable as crystals under nitrogen or argon atmosphere and can be stored for several weeks at room temperature. Its solid geometry and electronic structure were investigated by single crystal X-ray diffraction, electron paramagnetic resonance (EPR) spectroscopy, and superconducting quantum interferometer device (SQUID) measurements, in conjunction with theoretical calculations.

The temperature dependence of the magnetic susceptibility for a crystalline sample of  $I^{2+} \cdot 2[\text{Al}(\text{OR}_{\text{Me}})_4]^-$  was investigated (Figure 1).  $\chi_M T$  shows a slight decrease from 350 K up to 0.22  $\text{cm}^3 \cdot \text{K}/\text{mol}$  at 121 K as the sample is cooled. It then suddenly decreases, up to a minimum at 110 K, followed by another gradual decrease until to zero. This behavior is similar to those of known nitrogen-incorporating diradical dications<sup>9</sup> and consistent with the antiferromagnetic exchange. More strikingly when the temperature is increased from 2 K back to high temperature, the  $\chi_M T$  curve is not followed, but a hysteresis was observed instead. The temperature at which  $\chi_M T$  decreases on

Received: June 8, 2016

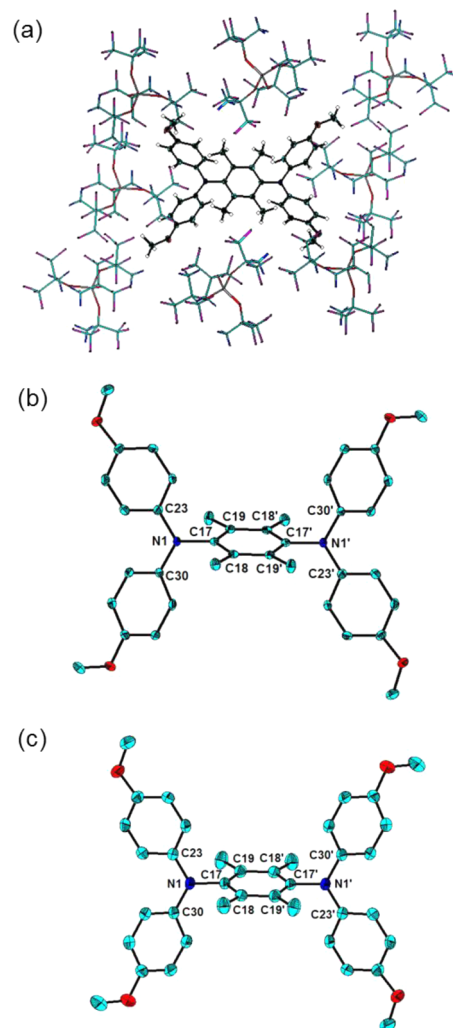
Published: August 1, 2016

Scheme 2. Synthesis of Compound 1 and Diradical Dication  $1^{2+}$ 

**Figure 1.** Temperature-dependent plots of  $\chi_M T$  for the crystals of  $1^{2+}$  recorded: (a) in the settle mode from 2–350 K; (b) in the sweep mode at the scan rate of 1 K  $\text{min}^{-1}$  from 100–150 K.

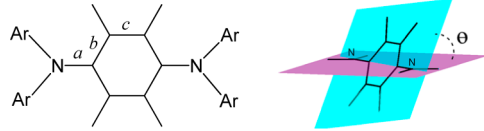
cooling ( $T_{1/2} = 118$  K) is 13 K lower than that at which  $\chi_M T$  increases when heating ( $T_{1/2} = 131$  K). The diradical of  $1^{2+}$  thus exhibits a 13 K wide hysteresis loop at the scan rate of 1 K  $\text{min}^{-1}$ , leading to magnetic bistability. We repeated the thermal cycle several times, but there is little change in the shape of the loop. The hysteresis width is scan-rate dependent and becomes wider at the faster temperature scan rates (Figure S2). The magnetic susceptibilities above and below the phase transition can be fitted with the Bleaney–Bowers equation.<sup>12</sup> The singlet–triplet gaps (or intramolecular exchange coupling constants) were estimated to be  $2J = -1.06$  kcal  $\text{mol}^{-1}$  for the low-temperature (LT) phase and  $-0.54$  kcal  $\text{mol}^{-1}$  for the high-temperature (HT) phase (Figure S3). The negative exchange coupling constants suggest singlet states for both phases, which can be thermally excited to their triplet excited states due to the small singlet–triplet energy gaps. The paramagnetism ( $\chi_M T = 0.70$   $\text{cm}^3 \cdot \text{K} / \text{mol}$ ) at 350 K corresponds to 93%  $S = 1$  Curie spins. Such a spin state conversion between two singlets in a discrete radical is distinct from previously reported magnetic bistability between a radical ( $S = 1/2$ ) and a spinless dimer ( $S = 0$ ).<sup>2–5</sup>

To rationalize the magnetic property, the structure of  $1^{2+}$  was examined by single crystal X-ray diffraction at 100 (LT) and 200 K (HT), respectively. Crystals suitable for X-ray crystallographic studies were obtained by the solution of salt  $1^{2+} \cdot 2[\text{Al}(\text{OR}_{\text{Me}})_4]^-$  in  $\text{CH}_2\text{Cl}_2$ . Crystal packing of  $1^{2+} \cdot 2[\text{Al}(\text{OR}_{\text{Me}})_4]^-$  at 100 K and the structures of dication  $1^{2+}$  at different temperatures together with their important structural parameters are illustrated in Figure 2 and Table 1. The



**Figure 2.** (a) Crystal packing of  $1^{2+} \cdot 2[\text{Al}(\text{OR}_{\text{Me}})_4]^-$  at 100 K. (b) Thermal ellipsoid (50%) drawing of  $1^{2+}$  at 100 K (hydrogen atoms are not shown). Selected bond lengths (Å) and angles (deg): N1–C23 1.405(3), N1–C30 1.400(3), N1–C17 1.433(3), C17–C18 1.411(4), C17–C19 1.408(4), C18–C19' 1.394(4), C17–N1–C23 120.6(2), C17–N1–C30 119.6(2), C23–N1–C30 119.8(2). (c) Thermal ellipsoid (50%) drawing of  $1^{2+}$  at 200 K (hydrogen atoms are not shown). Selected bond lengths (Å) and angles (deg): N1–C23 1.401(4), N1–C30 1.401(4), N1–C17 1.443(4), C17–C18 1.406(5), C17–C19 1.400(5), C18–C19' 1.397(5), C17–N1–C23 120.2(3), C17–N1–C30 119.2(3), C23–N1–C30 120.6(3).

molecular packings for the LT and HT phases are almost the same. Dications of  $1^{2+}$  are completely separated by  $[\text{Al}(\text{OR}_{\text{Me}})_4]^-$  anions (Figure 2a) through  $\text{F} \cdots \text{H}$  hydrogen bonds (2.5–2.8 Å), without apparent changes from HT to LT. The structures of the dication in both phases have an inversion center with planar geometries about the nitrogen atoms. The intramolecular  $\text{N} \cdots \text{N}$  distance (5.6 Å) in one dication of  $1^{2+}$  is

Table 1. Energy, Bond length (Å), and Torsion Angle (°) for  $\mathbf{1}^{2+}$ 


	$\Delta E_{X-OS}^a$ kcal mol <sup>-1</sup>	<i>a</i> , bond N1–C17	<i>b</i> , average of bonds C17–C18 and C17–C19	<i>c</i> C19–C18'	BLA <sup>b</sup>	$\theta$
CS <sup>a,c</sup>	+8.1	1.420	1.426	1.399	0.027	58.63
X-ray (100 K, LT)	–	1.433(3)	1.410(4)	1.394(4)	0.016	58.12(9)
X-ray (200 K, HT)	–	1.443(4)	1.403(5)	1.397(5)	0.006	61.47(11)
OS <sup>a,c</sup>	0	1.451	1.410	1.410	0	71.74
T <sup>a,c</sup>	+0.4	1.453	1.409	1.411	–0.002	73.08

<sup>a</sup>X = CS (closed-shell singlet), OS (open-shell singlet), or T (triplet). <sup>b</sup>BLA = bond length alteration, i.e., the difference between the average of length of longitudinal bonds (*b*) and the average of length of transverse bonds (*c*) in bridging phenyl ring. <sup>c</sup>Calculated at the level of (U)B3LYP/6-31G(d).

much shorter than the closest intermolecular N...N distance (10.1 Å) between two dications. The length of bond N–C<sub>bridge</sub> (i.e., bond *a*) between nitrogen atom and bridging phenyl moiety is longer than that between nitrogen atom and peripheral aryl ring, which is in sharp contrast to previously reported nitrogen-incorporating diradical dications,<sup>9</sup> indicating that  $\mathbf{1}^{2+}$  may have considerable diradical character. Reduced bond-length alteration (BLA) of a bridging phenyl ring has been considered as a signature of diradical character in hydrocarbon diradicals,<sup>8–10</sup> which is the difference between average longitudinal bond (i.e., bond *b*, Table 1) and transverse bond (i.e., bond *c*) of the bridging phenyl ring in this work. There is a crucial difference between BLAs (0.016, LT; 0.006, HT) of two phases, but both are much less than that of Chichibabin's hydrocarbon (0.052), suggesting strong diradical character of  $\mathbf{1}^{2+}$  for both phases. The relatively longer N–C<sub>bridge</sub> bond length and smaller BLA in the HT phase are consistent with the stronger diradical character of  $\mathbf{1}^{2+}$  at the higher temperature, as shown by SQUID measurements. Notably the torsion angle ( $\theta$ ), defined as the angle between bridging phenyl ring and the plane about the nitrogen atom as illustrated in the figure above Table 1, shows a difference of 3.3° far above the error limits between two phases.

To further understand the electronic structures, we carried out theoretical calculations for species  $\mathbf{1}^{2+}$ .<sup>13</sup> Full geometry optimizations were performed at the (U)B3LYP/6-31G(d) level and the obtained stationary points were characterized by frequency calculations. The broken-symmetry approach was applied for open-shell singlet calculations, and spin contamination errors were corrected by approximate spin-projection method.<sup>14</sup> Energies, bond lengths and their BLAs in the averages of bonds of the optimized closed-shell singlet (CS), open-shell singlet (OS), and pure diradical triplet (T) are listed in Table 1. Calculation of energy gaps shows that  $\mathbf{1}^{2+}$  has an OS ground state, and the calculated singlet–triplet energy gap (–0.4 kcal mol<sup>-1</sup>) is well in agreement with the experimental value (–0.54 kcal/mol at HT phase) determined from SQUID measurements. The N–C<sub>bridge</sub> bond lengths, BLAs, and torsion angles ( $\theta$ ) of  $\mathbf{1}^{2+}$  at HT and LT are between those of OS and CS, with the geometry at HT phase closer to that of OS. The above discussion based on the comparison of singlet–triplet energy gaps, N–C<sub>bridge</sub> bond lengths, and BLAs clearly shows singlet states with intermediate diradical character for  $\mathbf{1}^{2+}$  both at HT and LT phases. Dication  $\mathbf{1}^{2+}$  is thus best described as a resonance hybrid of the quinoidal structure (i.e., CS) and the diradical structure (i.e., OS), with a greater tendency to

diradical structure for the HT phase. It is worth noting that the energy difference between two structures of  $\mathbf{1}^{2+}$  (0.79 kcal mol<sup>-1</sup>), based on single point calculations using the HT and LT X-ray data of  $\mathbf{1}^{2+}$  performed at the UB3LYP/6-311G(d,p) level, reasonably agrees with that (0.52 kcal mol<sup>-1</sup>) between two singlet–triplet energy gaps determined from SQUID measurements, indicating that the structural changes between HT and LT are mainly responsible for modulating the magnetic interactions.

The magnetic property of  $\mathbf{1}^{2+}$  is further supported by means of EPR spectroscopy, which display typical broaden triplet-state signals with different *g* factors for two phases (LT  $g_x = 2.0033$ ,  $g_y = 2.0022$ ,  $g_z = 2.0041$ ; HT  $g_x = g_y = 2.0035$ ,  $g_z = 2.0042$ ) and the forbidden  $\Delta m_s = \pm 2$  half-field absorptions (Figures 3a, S5,

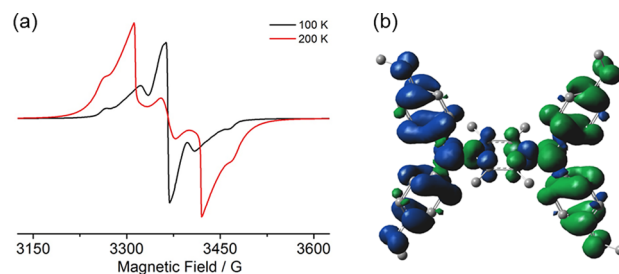


Figure 3. (a) Powder EPR spectra of  $\mathbf{1}^{2+}$  at 200 (in red) and 100 K (in black). (b) Electron spin density distribution of  $\mathbf{1}^{2+}$ -OS.

and S6).<sup>8,9</sup> The spin susceptibility determined by solid-state EPR as a function of temperature, i.e., the product (*IT*) of the intensity for the  $\Delta m_s = 2$  resonance and the temperature (*T*) vs *T* (Figure S7), shows a hysteresis loop similar to that observed by SQUID measurements (Figure 1). Zero-field parameters *D* (LT 10.50 mT, HT 10.20 mT) were determined by spectral simulation. The average spin–spin distance from *D* was estimated to be 6.4 Å for both phases, which is comparable to the distance (5.6 Å) between two N atoms in the X-ray structure, supporting the intramolecular electron-exchange interaction. The slightly longer spin–spin distance indicates that the unpaired electrons are more delocalized to the peripheral aryl ring systems, which is consistent with the electron spin density distribution map (Figure 3b).

We report the preparation and characterization of a nitrogen-containing diradical dication  $\mathbf{1}^{2+}$ , which exhibits a phase transition with a thermal hysteresis loop over the temperature range 118–131 K, indicating magnetic bistability. The phases

above and below the loop correspond to two singlet states of the diradical dication with different electron-exchange coupling constants. Crystal structural analysis, EPR simulation, and theoretical calculations indicate that the magnetic bistability is mainly caused by intramolecular electron-exchange interactions. The work provided an unprecedented magnetic bistable material to be used in the design of electronic devices. A new class of organic analogues of metal ion-based spin crossover complexes may be accessible by rational designs of discrete magnetic bistable diradicals.

## ■ ASSOCIATED CONTENT

### Supporting Information

The Supporting Information is available free of charge on the ACS Publications website at DOI: 10.1021/jacs.6b05863.

Experimental section, cyclic voltammogram of **1**, EPR spectra, and theoretical calculations (PDF)

Crystallographic data (CIF)

Crystallographic data (CIF)

## ■ AUTHOR INFORMATION

### Corresponding Author

\*xpwang@nju.edu.cn

### Notes

The authors declare no competing financial interest.

## ■ ACKNOWLEDGMENTS

We thank the National Natural Science Foundation of China (grants 21525102, X.P., and 21171089, Y. S.), the Major State Basic Research Development Program (2016YFA0300404, X.P.), and the Natural Science Foundation of Jiangsu Province (Grant BK20140014, X.P.) for financial support. We are grateful to the High Performance Computing Center of Nanjing University for doing the numerical calculations in this paper on its IBM Blade cluster system.

## ■ REFERENCES

- (1) (a) Rajca, A. *Chem. Rev.* **1994**, *94*, 871. (b) Schmittel, M.; Burghart, A. *Angew. Chem., Int. Ed. Engl.* **1997**, *36*, 2550. (c) Nishinaga, T.; Komatsu, K. *Org. Biomol. Chem.* **2005**, *3*, 561. (d) Hicks, R. G. *Org. Biomol. Chem.* **2006**, *5*, 1321. (e) Hankache, J.; Wenger, O. S. *Chem. Rev.* **2011**, *111*, 5138. (f) Mas-Torrent, M.; Crivillers, N.; Rovira, C.; Veciana, J. *Chem. Rev.* **2012**, *112*, 2506. (g) Heckmann, A.; Lambert, C. *Angew. Chem., Int. Ed.* **2012**, *51*, 326. (h) Abe, M. *Chem. Rev.* **2013**, *113*, 7011.
- (2) (a) Barclay, T. M.; Cordes, A. W.; George, N. A.; Haddon, R. C.; Itkis, M. E.; Mashuta, M. S.; Oakley, R. T.; Patenaude, G. W.; Reed, R. W.; Richardson, J. F.; Zhang, H. *J. Am. Chem. Soc.* **1998**, *120*, 352. (b) Brusso, J. L.; Clements, O. P.; Haddon, R. C.; Itkis, M. E.; Leitch, A. A.; Oakley, R. T.; Reed, R. W.; Richardson, J. F. *J. Am. Chem. Soc.* **2004**, *126*, 8256. (c) Brusso, J. L.; Clements, O. P.; Haddon, R. C.; Itkis, M. E.; Leitch, A. A.; Oakley, R. T.; Reed, R. W.; Richardson, J. F. *J. Am. Chem. Soc.* **2004**, *126*, 14692. (d) Alberola, A.; Collis, R. J.; Humphrey, S. M.; Less, R. J.; Rawson, J. M. *Inorg. Chem.* **2006**, *45*, 1903. (e) Alberola, A.; Eisler, D. J.; Harvey, L.; Rawson, J. M. *CrystEngComm* **2011**, *13*, 1794.
- (3) (a) Fujita, W.; Awaga, K. *Science* **1999**, *286*, 261. (b) McManus, G. D.; Rawson, J. M.; Feeder, N.; van Duijn, J.; McInnes, E. J. L.; Novoa, J. J.; Burriel, R.; Palacio, F.; Olliete, P. *J. Mater. Chem.* **2001**, *11*, 1992. (c) Fujita, W.; Awaga, K.; Matsuzaki, H.; Okamoto, H. *Phys. Rev. B: Condens. Matter Mater. Phys.* **2002**, *65*, 064434. (d) Vela, S.; Mota, F.; Deumal, M.; Suizu, R.; Shuku, Y.; Mizuno, A.; Awaga, K.; Shiga, M.; Novoa, J. J.; Riba-Arino, J. *Nat. Commun.* **2014**, *5*, 4411.

(4) Itkis, M. E.; Chi, X.; Cordes, A. W.; Haddon, R. C. *Science* **2002**, *296*, 1443.

(5) (a) Robertson, C. M.; Leltch, A. A.; Cvrkalj, K.; Reed, R. W.; Myles, D. J. T.; Dube, P. A.; Oakley, R. T. *J. Am. Chem. Soc.* **2008**, *130*, 8414. (b) Lekin, K.; Winter, S. M.; Downie, L. E.; Bao, X.; Tse, J. S.; Desgreniers, S.; Secco, R. A.; Dube, P. A.; Oakley, R. T. *J. Am. Chem. Soc.* **2010**, *132*, 16212. (c) Lekin, K.; Phan, H.; Winter, S. M.; Wong, J. W. L.; Leitch, A. A.; Laniel, D.; Yong, W.; Secco, R. A.; Tse, J. S.; Desgreniers, S.; Dube, P. A.; Shatruk, M.; Oakley, R. T. *J. Am. Chem. Soc.* **2014**, *136*, 8050.

(6) (a) Shultz, D. A.; Fico, R. M., Jr.; Boyle, P. D.; Kampf, J. W. *J. Am. Chem. Soc.* **2001**, *123*, 10403. (b) Shultz, D. A.; Fico, R. M., Jr.; Pinkerton, A. A.; Boyle, P. D. *J. Am. Chem. Soc.* **2003**, *125*, 15426.

(7) (a) Kahn, O.; Martinez, C. J. *Science* **1998**, *279*, 44. (b) Halcrow, M. A. *Spin-Crossover Materials. Properties and Applications*; Wiley & Sons: Chichester, 2013. (c) Brooker, S. *Chem. Soc. Rev.* **2015**, *44*, 2880.

(8) (a) Nelsen, S. F.; Ismagilov, R. F.; Powell, D. R. *J. Am. Chem. Soc.* **1997**, *119*, 10213. (b) Ito, A.; Urabe, M.; Tanaka, K. *Angew. Chem., Int. Ed.* **2003**, *42*, 921. (c) Völker, S. F.; Renz, M.; Kaupp, M.; Lambert, C. *Chem. - Eur. J.* **2011**, *17*, 14147. (d) Yokoyama, Y.; Sakamaki, D.; Ito, A.; Tanaka, K.; Shiro, M. *Angew. Chem., Int. Ed.* **2012**, *51*, 9403. (e) Kamada, K.; Fuku-en, S.; Minamide, S.; Ohta, K.; Kishi, R.; Nakano, M.; Matsuzaki, H.; Okamoto, H.; Higashikawa, H.; Inoue, K.; Kojima, S.; Yamamoto, Y. *J. Am. Chem. Soc.* **2013**, *135*, 232.

(9) (a) Zheng, X.; Wang, X.; Qiu, Y.; Li, Y.; Zhou, C.; Sui, Y.; Li, Y.; Ma, J.; Wang, X. *J. Am. Chem. Soc.* **2013**, *135*, 14912. (b) Su, Y.; Wang, X.; Zheng, X.; Zhang, Z.; Song, Y.; Sui, Y.; Li, Y.; Wang, X. *Angew. Chem., Int. Ed.* **2014**, *53*, 2857. (c) Wang, X.; Zhang, Z.; Song, Y.; Su, Y.; Wang, X. *Chem. Commun.* **2015**, *51*, 11822. (d) Su, Y.; Wang, X.; Li, Y.; Song, Y.; Sui, Y.; Wang, X. *Angew. Chem., Int. Ed.* **2015**, *54*, 1634.

(10) (a) Tschitschibabin, A. E. *Ber. Dtsch. Chem. Ges.* **1907**, *40*, 1810. (b) Montgomery, L. K.; Huffman, J. C.; Jurczak, E. A.; Grendze, M. P. *J. Am. Chem. Soc.* **1986**, *108*, 6004 and references therein. (c) Müller, E.; Pfanz, H. *Ber. Dtsch. Chem. Ges. B* **1941**, *74*, 1051. (d) Schmidt, H.; Brauer, H.-D. *Angew. Chem., Int. Ed. Engl.* **1971**, *10*, 506.

(11) Krossing, I. *Chem. - Eur. J.* **2001**, *7*, 490.

(12) Bleaney, B.; Bowers, K. D. *Proc. R. Soc. London, Ser. A* **1952**, *214*, 451.

(13) All calculations were performed using: Frisch, M. J.; Trucks, G. W.; Schlegel, H. B.; Scuseria, G. E.; Robb, M. A.; Cheeseman, J. R.; Scalmani, G.; Barone, V.; Mennucci, B.; Petersson, G. A.; Nakatsuji, H.; Caricato, M.; Li, X.; Hratchian, H. P.; Izmaylov, A. F.; Bloino, J.; Zheng, G.; Sonnenberg, J. L.; Hada, M.; Ehara, M.; Toyota, K.; Fukuda, R.; Hasegawa, J.; Ishida, M.; Nakajima, T.; Honda, Y.; Kitao, O.; Nakai, H.; Vreven, T.; Montgomery, J. A., Jr.; Peralta, J. E.; Ogliaro, F.; Bearpark, M.; Heyd, J. J.; Brothers, E.; Kudin, K. N.; Staroverov, V. N.; Kieth, T.; Kobayashi, R.; Normand, J.; Raghavachari, K.; Rendell, A.; Burant, J. C.; Iyengar, S. S.; Tomasi, J.; Cossi, M.; Rega, N.; Millam, N. J.; Klene, M.; Knox, J. E.; Cross, J. B.; Bakken, V.; Adamo, C.; Jaramillo, J.; Gomperts, R.; Stratmann, R. E.; Yazyev, O.; Austin, A. J.; Cammi, R.; Pomelli, C.; Ochterski, J. W.; Martin, R. L.; Morokuma, K.; Zakrzewski, V. G.; Voth, G. A.; Salvador, P.; Dannenberg, J. J.; Dapprich, S.; Daniels, A. D.; Farkas, Ö.; Foresman, J. B.; Ortiz, J. V.; Cioslowski, J.; Fox, D. J. *Gaussian 09*, revision B.01; Gaussian, Inc.: Wallingford CT, 2010.

(14) Kitagawa, Y.; Saito, T.; Ito, M.; Shoji, M.; Koizumi, K.; Yamanaka, S.; Kawakami, T.; Okumura, M.; Yamaguchi, K. *Chem. Phys. Lett.* **2007**, *442*, 445.